Chinese Chemical Letters 33 (2022) 3549–3555

Contents lists available at ScienceDirect

Chinese Chemical Letters

journal homepage: www.elsevier.com/locate/cclet

Experimental and theoretical insights into copper phthalocyanine-based covalent organic frameworks for highly efficient radioactive iodine capture

Xuewei Liu[a], Anrui Zhang[a], Ran Ma[a], Bo Wu[a], Tao Wen[a,*], Yuejie Ai[a], Mingtai Sun[b], Jie Jin[a], Suhua Wang[a,b], Xiangke Wang[a,*]

[a] MOE Key Laboratory of Resources and Environmental Systems Optimization, College of Environment and Chemical Engineering, North China Electric Power University, Beijing 102206, China
[b] Guangdong Provincial Key Laboratory of Petrochemical Pollution Process and Control, School of Environmental Science and Engineering, Guangdong University of Petrochemical Technology, Maoming 525000, China

ARTICLE INFO

Article history:
Received 7 December 2021
Revised 28 February 2022
Accepted 1 March 2022
Available online 4 March 2022

Keywords:
Cu_xPc-COFs
Microwave
Iodine adsorption
Charge transfer
Electrostatic interaction

ABSTRACT

Exploring efficient materials for capturing radioactive iodine in nuclear waste is of great significance for the progress of nuclear energy as well as the protection of ecological environment. Covalent organic frameworks (COFs) have emerged as promising adsorbents because of their predesignable and functionalizable skeleton structures. However, it remains a grand challenge to achieve large scale preparation of COFs. In this work, we developed a mild and efficient microwave irradiation method instead of the traditional solvothermal method to prepare copper phthalocyanine-based covalent organic frameworks (Cu_xPc-COFs) within only 15 min. The nitrogen-rich 1,2,4,5-tetracarbonitrilebenzene (TCNB) was selected as the solely organic ligand to construct copper phthalocyanine-based 2D conjugated COFs. The resultant Cu_xPc-COFs exhibited excellent iodine enrichment with 2.99 g/g for volatile iodine and 492.27 mg/g for iodine-cyclohexane solution, respectively, outperforming that of many porous materials. As indicated by spectroscopic analysis and DFT calculations, this impressive adsorption performance can be attributed to the charge transfer arising from nitrogen-rich phthalocyanine structures and electron-rich π-conjugated systems with iodine molecules. Moreover, the strong electrostatic interaction between Cu(II) on chelate centers and polyiodide anions (I_x^-) also play an important role in the firmly trapping radioactive iodine. Therefore, this study provides a facile and intelligent approach to implement metal-based COFs for the remediation of toxic radioactive iodine.

As a kind of clean and efficient new energy, nuclear energy is of great significance to meet the demand of energy and solve the problems of environmental pollution [1,2]. From the standpoints of sustainable development strategy, nuclear energy and nuclear fuel treatment require strict management and safeguards, which means that it is necessary to recover and remove hazardous radionuclides from nuclear waste. Of these, radioiodine (^{129}I and ^{131}I) is one of the most typical and harmful radioactive emissions in nuclear waste. In particular, ^{129}I has an enormously long radioactive half-life (1.57×10^7 years), and it is easy to volatilize and diffuse into the air, posing great harm to the ecological environment [3]. While ^{131}I, as alternative stable iodine, can participate in the metabolism of iodine in the human body and quickly accumulate in the thyroid through blood circulation, resulting in thyroid injury and even carcinogenesis, as evidenced by the increased incidence of thyroid cancer after the Chernobyl accident [4]. The accident at Fukushima once again poses a threat to human health and the ecological environment [5,6], so it is crucial to design and fabricate advanced materials that can capture and store iodine effectively.

Currently, the leading approach of treating radioiodine in vapor waste is to use stable silver-containing zeolites for adsorption [7,8]. Although silver-containing zeolites have a high removal rate of radioiodine, the reaction between iodine and silver is irreversible. And the utilization of noble silver will lead to increase its cost for iodine capture. Compared with silver, copper has lower molecular weight and is more economical. What is more, copper still possesses a high affinity for iodine (CuI $K_{sp} = 1.10 \times 10^{-12}$) [9]. Considering the excellent coordination ability of copper, it can form

* Corresponding authors.
E-mail addresses: twen@ncepu.edu.cn (T. Wen), xkwang@ncepu.edu.cn (X. Wang).

https://doi.org/10.1016/j.cclet.2022.03.001
1001-8417/

copper coordination compounds with a variety of ligands containing nitrogen and oxygen [9–12]. Therefore, it would be very attractive to choose specific materials containing Cu as highly efficient iodine adsorbents. Seeking highly efficient iodine adsorbents from cheap and environmentally friendly, researchers have designed a variety of materials (such as activated carbon [13], aerogels [14], LDHs [15], silicon materials [16], metal organic frameworks [17,18], covalent organic frameworks [19]) and evaluated their iodine capture performance.

Covalent organic frameworks (COFs) are an emerging class of porous crystalline materials, which are built from organic monomers via strong covalent linkages [20–22]. COFs possess excellent integrating physicochemical properties such as high thermal stability, large specific surface area and abundant pores. In addition, the skeleton structures of COFs are highly ordered, predesignable and functionalizable, and the active sites can be precisely integrated into the framework matrix in a specific way [23]. Owing to their comprehensive features, the class of COFs can provide an attractive alternative platform for radionuclide sequestration. However, the successful construction of COFs is still a great challenge. Nowadays, most of the synthesized COFs are achieved by the solvothermal method, which is found to be maintained at high temperature for a long time during the synthesis process. Compared with traditional heating method, microwave radiation produces efficient internal heating by directly coupling microwave energy with molecules (solvents, reagents and catalysts) in the reaction mixture [24]. Microwave technology has been widely used in the synthesis of many compounds due to its advantages such as accelerated reaction time, higher yields and cleaner products, so it can be a powerful strategy to replace solvothermal synthesis. For example, Campbell *et al.* successfully prepared boronate-ester linked COFs (COF-5 and COF-102) by a mild microwave synthesis method [25]. Impressively, the physical properties of these COFs were comparable to the materials prepared by solvothermal synthesis, whereas the synthesis rate of this method was 200 times faster than that of solvothermal synthesis. To the best of our knowledge, studies of COFs prepared by microwave synthesis method have rarely been reported. Therefore, it is of great research value and application prospect to explore the microwave synthesis method in the field of COFs.

According to the previous studies, it is considered that there is an intense interaction between nitrogen atoms and iodine molecules, which is significantly conducive to adsorption [26]. What is more, the electron-rich π-conjugated systems (like aromatic rings) in the material structure can also provide abundant adsorption sites, thereby improving the affinity of absorbents to iodine molecules [27]. Inspired by this point, herein, a novel microwave synthesis method was developed to rapidly synthesize large quantities of copper phthalocyanine-covalent organic frameworks (Cu_xPc-COFs) materials ($Cu_{0.5}$Pc-COF, $Cu_{0.25}$Pc-COF and $Cu_{0.125}$Pc-COF). Nitrogen-rich 1,2,4,5-tetracarbonitrile benzene (TCNB) was selected as the solely organic building block, and Cu(II) was anchored at the coordination center, resulting in a stable conjugated two-dimensional network with single-atomic centers with assistance of microwave irradiation, as illustrated in Scheme 1. Such Cu_xPc-COFs not only have nitrogen-rich structures and π-conjugate systems, but also have Cu coordination centers with a strong affinity for iodine. Furthermore, we systematically explored the adsorption performance of Cu_xPc-COFs toward volatile iodine and iodine from cyclohexane solution in terms of adsorption kinetics and capacities. Especially, the optimal $Cu_{0.25}$Pc-COF exhibited excellent iodine enrichment capacity (2.99 g/g for iodine vapor and 492.27 mg/g for iodine solution). More importantly, the rationality of interaction mechanism was fundamentally elucidated by morphologic and spectroscopic analyses of iodine-laden $Cu_{0.25}$Pc-COF. Density functional theory (DFT) calculations more clearly illustrated the strong interaction between I_2 and Cu_xPc-COFs. As expected, Cu_xPc-COFs are considered to be a promising type of host material for radioactive iodine uptake from the nuclear waste due to its two-dimensional conjugate network with rigid structures and uneven charged coordinated copper centers.

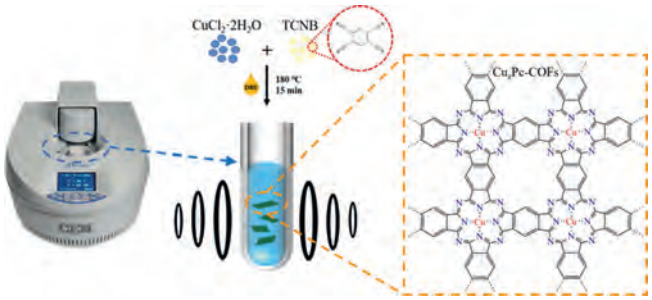

Scheme 1. Schematic illustration for the synthesis of Cu_xPc-COFs.

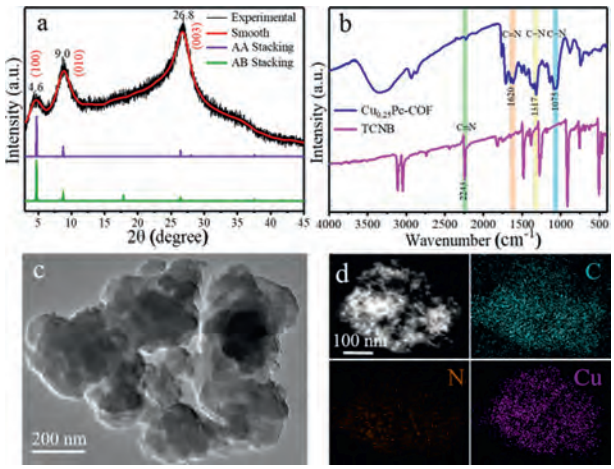

Fig. 1. (a) PXRD pattern of $Cu_{0.25}$Pc-COF. (b) FT-IR spectra of $Cu_{0.25}$Pc-COF and TCNB. (c) HRTEM image of $Cu_{0.25}$Pc-COF. (d) Elemental mapping images of C, N and Cu for $Cu_{0.25}$Pc-COF.

To analyze the crystal structures of as-synthesized Cu_xPc-COFs, powder X-ray diffraction (PXRD) was conducted (Fig. 1a and Fig. S1 in Supporting information). As shown in Fig. S1, the PXRD patterns of three Cu_xPc-COFs exhibited similar diffraction patterns from $2\theta = 3°$ up to 30°, indicating that the amount of copper ions did not change the crystallinity of the COFs during the synthesis process. As represented in Fig. 1a, the peaks appearing at $2\theta = 4.6°$ and 8.2° in the low-angle region were related to the (100) and (010) facets of orthorhombic lattice, which were consistent with reported literature [28]. A strong peak at $2\theta = 26.8°$ corresponded to the (001) diffraction, indicating the presence of the π-π stacking of 2D layers along the *c* direction. In order to clearly illustrate the constitution of Cu_xPc-COFs, we used Materials Studio to construct structural models and simulated two stacking possibilities: AA eclipsed and AB staggered models. Through the Pawley refinement studies, it could be observed that the PXRD pattern generated by eclipsed AA-stacking mode was more similar to the experimental pattern. However, with the increasing amount of Cu^{2+}, the characteristic diffraction peaks of Cu^0 appeared in the case of $Cu_{0.5}$Pc-COF, which was mainly due to the reduction of excess Cu^{2+} to Cu^0 in the presence of ethylene glycol. Moreover, Fourier transform infrared (FT-IR) spectra clearly revealed the change of the functional groups during the synthesis process (Fig. 1b and Fig. S2 in Supporting information). Compared with the infrared spectra of $Cu_{0.25}$Pc-COF and TCNB precursor, the characteristic vibration peak of C≡N (2243 cm^{-1}) representing cyanide groups dis-

appeared completely, while the stretching vibration peaks of C=N (1620 cm^{-1}) and C−N (1075 and 1319 cm^{-1}) emerged, which was indicative of a successful polymerization reaction [29,30]. The morphology of the as-prepared $Cu_{0.25}$Pc-COF was investigated by scanning electron microscopy (SEM, Fig. S3 in Supporting information), showing an aggregation of irregular massive particles with smooth surface. Moreover, the high-resolution transmission electron microscopy (HRTEM, Fig. 1c) characterization clearly revealed its layered structures, and no visible Cu nanoparticles were observed. The corresponding energy-dispersive X-ray spectroscopy (EDS, Fig. 1d) mapping suggested that C, N and Cu elements were uniformly distributed over the surface of $Cu_{0.25}$Pc-COF, signifying that the Cu(II) species were highly dispersed in the $Cu_{0.25}$Pc-COF network. However, the results showed that the content of N element was lower than that of Cu, which might be attributed to the elimination of cyanide groups (−C≡N) as well as the partial decomposition of linkers in the frameworks [31,32].

N_2 adsorption and desorption analyses were used to evaluate the porosity and surface areas of Cu_xPc-COFs. The Brunauer-Emmett-Teller (BET) surface areas were found to be 37.32 m^2/g for $Cu_{0.5}$Pc-COF, 19.82 m^2/g for $Cu_{0.25}$Pc-COF and 9.31 m^2/g for $Cu_{0.125}$Pc-COF (Fig. S4a in Supporting information). The low specific surface areas of Cu_xPc-COFs are mainly limited by the coordination of Cu center occupying the pore space, resulting in the imperfect crystallinity of the materials or the solvent (ethylene glycol) could be trapped in the COFs [33,34]. According to the pore-size distribution (Fig. S4b in Supporting information), the presence of mesopores (2.6 nm) was evident in Cu_xPc-COFs. With the increasing amount of copper ions, the specific surface areas accordingly increased, but the pore size distributions did not change, which was probably caused by the generated Cu° nanoparticles with a certain specific surface area [35]. In order to check the thermal stability of as-synthesized materials, we further performed the thermogravimetric analysis (TGA) under N_2 atmosphere. It could be observed from the TGA profiles (Fig. S5 in Supporting information) that after the loss of approximately 2-3 wt% ambient water (<100 °C), Cu_xPc-COFs presented a weight loss of 10%-15% without obvious decomposition even up to 400 °C, indicating the high thermal stability of Cu_xPc-COFs.

As the structures of Cu_xPc-COFs possess high nitrogen content and contain abundant π-conjugated systems, such unique Cu_xPc-COFs network is beneficial for the adsorption of volatile iodine [27,36]. Moreover, on the basis of their excellent thermal stability, Cu_xPc-COFs are suitable for the experiments of volatile iodine adsorption by using the gravimetric method. Specifically, the desired Cu_xPc-COFs powder and excess nonradioactive iodine pellets were placed into a hermetic system at 80 °C and ambient pressure, and the adsorption capacities were obtained by measuring the weight change of the samples before and after adsorption. As shown in Fig. 2a, the iodine loading amounts on Cu_xPc-COFs increased with the reaction time and tended to become equilibrium. Specifically, the adsorption rates of iodine by Cu_xPc-COFs were considerably fast within the initial contact of 8 h, reaching more than 80% of the total adsorption capacities. After 48 h, it was noteworthy that the iodine-capture capacity of $Cu_{0.25}$Pc-COF was 2.99 g/g, which was higher than those of $Cu_{0.125}$Pc-COF (2.66 g/g) and $Cu_{0.5}$Pc-COF (2.40 g/g). Interestingly, the adsorption capacities of Cu_xPc-COFs toward volatile iodine did not increase with the increase of copper content. It was speculated that the presence of Cu° in $Cu_{0.5}$Pc-COF, as confirmed by the result of PXRD analysis, occupied the binding sites of solid particles and prevented the further penetration or diffusion of volatile iodine from the exterior particle surface to π-conjugated interior. Therefore, the higher the proportion of Cu°, the lower the proportion of COFs with more active sites, which was not conducive to the adsorption of volatile iodine. As a result, $Cu_{0.25}$Pc-COF with plentiful ordered N-coordinated Cu atoms gave the highest adsorption value among the synthetic Cu_xPc-COF materials. Interestingly, the kinetic data could be analyzed according to the pseudo-second-order kinetic model (Fig. 2b and Table 1), which could be described by Eq. 1:

$$\frac{t}{Q_t} = \frac{1}{kQ_e^2} + \frac{t}{Q_e} \quad (1)$$

herein, t is adsorption time (h). Q_e and Q_t are the adsorption amounts of iodine at equilibrium and at time t (mg/g), respectively. And k is the pseudo-second-order rate constant of adsorption (g mg^{-1} h^{-1}). The obtained high correlation coefficients (R^2 > 0.999) demonstrated that the adsorption of iodine on Cu_xPc-COFs conformed to the *pseudo*-second-order kinetic model, indicating that chemical adsorption was the dominant process [36,37]. Remarkably, the iodine-capture performance of $Cu_{0.25}$Pc-COF was superior to that exhibited by state-of-the-art porous adsorbents (Fig. 2c and Table 2) [27,38–48].

The above results proved that $Cu_{0.25}$Pc-COF had an excellent ability to adsorb volatile iodine, and we further studied its adsorption of iodine from solution. Considering that nonpolar iodine is difficult to dissolve in polar solvents such as water, cyclohexane was selected as solvent for the batch adsorption experiments, and UV-vis spectroscopy was used to detect the concentration of iodine in solution. By changing the initial iodine concentrations in cyclohexane solution, the functional relationship between the amount of iodine adsorbed by $Cu_{0.25}$Pc-COF adsorbent and the iodine concentrations at equilibrium was determined. As we all known, the adsorption equilibrium isotherm is used to describe the diffusion of adsorbates molecules and adsorbents at equilibrium [31]. In order to evaluate the adsorption capacity of $Cu_{0.25}$Pc-COF for iodine, equilibrium data were collected after exposure to iodine cyclohexane solution with the initial concentrations in the range of 0.25-10 g/L. As can be seen from Fig. 2d, a continuous increase of iodine adsorption with augmentation of the equilibrium concentrations was observed. The adsorption isotherms could be simulated by two

Table 1
The pseudo-second-order kinetic data of the iodine adsorption of Cu_xPc-COFs.

Samples	Q_e (exp) (g/g)	Q_e (g/g)	k (h^{-1})	R^2
$Cu_{0.5}$Pc-COF	2.66	2.78	0.1788	0.9996
$Cu_{0.25}$Pc-COF	2.99	3.19	0.1019	0.9991
$Cu_{0.125}$Pc-COF	2.40	2.53	0.1730	0.9992

Table 2
Comparison of iodine adsorption capacities of this Cu_xPc-COFs with other reported adsorbents.

Materials	Temp. (°C)	Equilibrium time	Capacity (g/g)	Ref.
HKUST-1@PES	75	~33 h	0.538	38
Cu-BTC@PES	75	~75 h	0.639	39
NUC-5	~77	7 h	0.776	40
JUC-Z2	25	~100 min	1.44	41
NU-1000	80	~48 h	1.45	42
Cu-BTC	75	9 h	1.75	43
TTPT	~77	~24 h	1.77	44
PAF-1	25	~100 min	1.86	41
NiP-CMP	~77	~12 h	2.02	45
CMPN-3	~70	1 h	2.08	46
MOF-808	80	~48 h	2.18	42
BDP-CPP-2	75	~8 h	2.23	47
$Cu_{0.125}$Pc-COF	80	~24 h	2.40	This work
PAF-25	75	48 h	2.60	27
$Cu_{0.5}$Pc-COF	80	~24 h	2.66	This work
PAF-23	75	48 h	2.71	27
PAF-24	75	48 h	2.76	27
BDP-CPP-1	75	~8 h	2.83	47
AzoPPN	~77	48 h	2.90	48
$Cu_{0.25}$Pc-COF	80	~24 h	2.99	This work

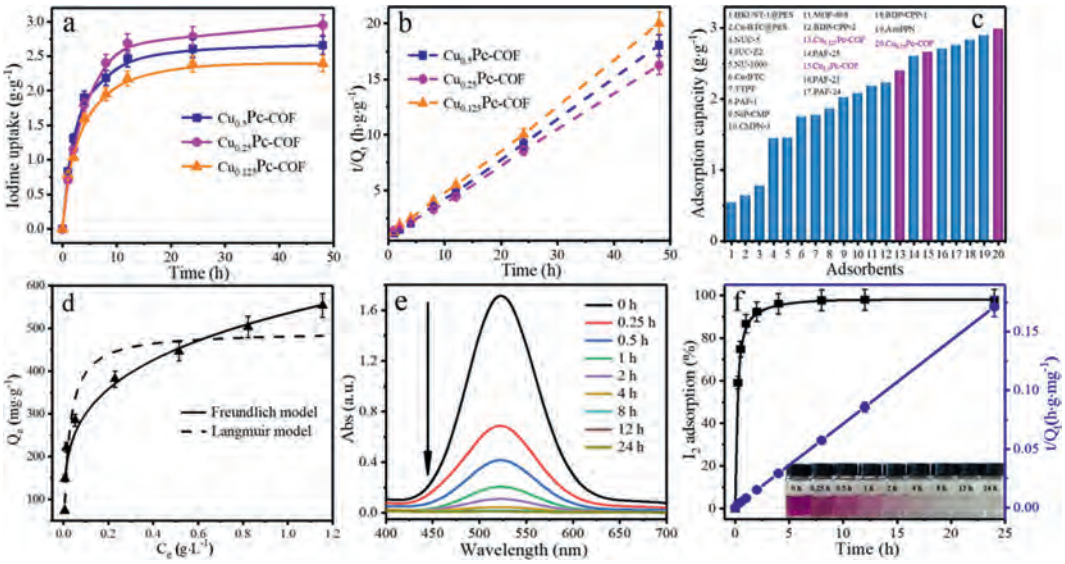

Fig. 2. (a) Gravimetric iodine uptake of Cu_xPc-COFs as a function of time at 80 °C and ambient pressure. (b) The *pseudo*-second-order kinetic data of the iodine adsorption of Cu_xPc-COFs. (c) Comparisons of iodine adsorption capacities for Cu_xPc-COFs with other different porous materials. The pink columns represent the new synthetic Cu_xPc-COFs in this work, and the blue columns represent the other porous materials. (d) Langmuir and Freundlich models fitting of $Cu_{0.25}$Pc-COF adsorption isotherm of iodine in cyclohexane solution (contact time is 24 h, $T = 298$ K). (e) UV-vis absorption spectra of iodine-cyclohexane solution at different adsorption times. (f) Kinetics of the iodine adsorption process on $Cu_{0.25}$Pc-COF plotted as the relative removal amount of iodine (%) (black line) and the plot of t/Q_t (blue line) *vs.* the time (initial iodine concentration is 0.5 g/L, $T = 298$ K). Inset: the photograph displays the removal effect of $Cu_{0.25}$Pc-COF on iodine-cyclohexane solution at different times.

typical Langmuir and Freundlich models. The Langmuir isotherm model assumes that the adsorption on the surface of adsorbent is uniform and monolayer, while the Freundlich model assumes that adsorption processes take place over the heterogeneous surface, and the specific formulas are as follows:

$$\text{Langmuir model: } Q_e = \frac{Q_m K_L C_e}{1 + K_L C_e} \quad (2)$$

$$\text{Freundlich model: } Q_e = K_F C_e^{\frac{1}{n}} \quad (3)$$

where Q_m and Q_e are the maximum adsorption capacity and the amounts of iodine adsorbed on the adsorbent at equilibrium (mg/g). C_e is the equilibrium concentration of iodine in cyclohexane solution (mg/L). K_L and K_F are the Langmuir constant relating to the adsorption heat and the Freundlich constant representing the adsorption capacity when equilibrium concentration is equal to 1. And $1/n$ refers to the adsorption intensity. The corresponding constants of the two isotherm models were listed in Table S1 (Supporting information). One can see from the R^2 values that the Freundlich model fitted the data better than the Langmuir model, which implied the heterogeneous distribution of adsorptive sites on the surface of $Cu_{0.25}$Pc-COF [49]. In addition, n value was found to be 3.44 (between 1 and 10), representing the good affinity of $Cu_{0.25}$Pc-COF toward iodine. On the basis of the Langmuir model, the saturation adsorption capacity was calculated to be 492.27 mg/g, which exceeded that for reported H-C-CTPs (293 mg/g) [50], NiP-CMP (326 mg/g) [45] and Cu/MIL-101 (432 mg/g) [51].

The adsorption kinetics of iodine was further investigated. It was found that the concentrations of iodine in the solution (initial iodine concentration was 0.5 g/L) decreased rapidly with the increasing contact time: the relative removal amount of iodine reached 60% within 0.25 h and increased to 98% after prolonging the contact time to 8 h (Figs. 2e and f). From the inset of Fig. 2f, it was evident that the color of the solutions changed from dark purple to light purple and finally to colorless as the time progressed. It was worth mentioning that $Cu_{0.25}$Pc-COF gave an h (kQ_e^2) value as high as 325.06 mg g^{-1} h^{-1}, representing a high adsorption rate. The plot of t/Q_t *vs.* t of the kinetic data exhibited a perfect linear relationship ($R^2 = 0.9999$), which proved that the kinetic data fitted well with the pseudo-second-order kinetic model. Therefore, the rate-limiting step of the adsorption process was chemical adsorption [49].

A series of characterization techniques were adopted to explore the interaction mechanism between Cu_xPc-COFs and iodine. We firstly employed PXRD to detect the crystal changes of the three materials before and after iodine adsorption (Fig. S6 in Supporting information). It could be observed that several new peaks appeared as typical CuI features in the PXRD pattern of $Cu_{0.5}$Pc-COF, which was mainly due to the redox reaction between excess Cu^0 and iodine molecules with the assistance of reaction temperature (80 °C). The weak intense peaks of CuI in the PXRD pattern of $Cu_{0.25}$Pc-COF confirmed that partial Cu atoms were still anchored on the $Cu_{0.25}$Pc-COF matrix. The PXRD patterns of $Cu_{0.25}$Pc-COF after adsorbing iodine vapor and iodine-cyclohexane solution were shown in Fig. 3a. Interestingly, unlike that after adsorption of iodine vapor, the characteristic diffraction peaks of CuI crystal were absent in the PXRD pattern of $Cu_{0.25}$Pc-COF after adsorption of 3.0 g/L iodine-cyclohexane solution, probably on the account that the adsorption environment in solution (25 °C) was milder than that in iodine vapor (80 °C). It was worth noting that compared with the pristine sample, the partial characteristic peaks disappeared in the PXRD patterns of $Cu_{0.25}$Pc-COF-I_2. This phenomenon indicated that the adsorption behavior of iodine could cause some distortion of the phthalocyanine structure of $Cu_{0.25}$Pc-COF. In order to further study the influence of adsorption behavior on the structure of COFs, the desorption experiments were carried out by soaking I_2-laden $Cu_{0.25}$Pc-COF in ethanol and subsequent 1 mol/L HCl solution. As can be seen from PXRD patterns in Fig. S7 (Supporting information), the strong diffraction peak at $2\theta = 26.8°$ corresponding to the (001) diffraction still existed, indicating that the π-π stacking structure of the 2D layers was not destroyed after iodine adsorption. However, the peak at $2\theta = 4.6°$ was obviously weakened, which proved that the adsorption of iodine had a great impact on the crystallinity of the materials due to the continuous oc-

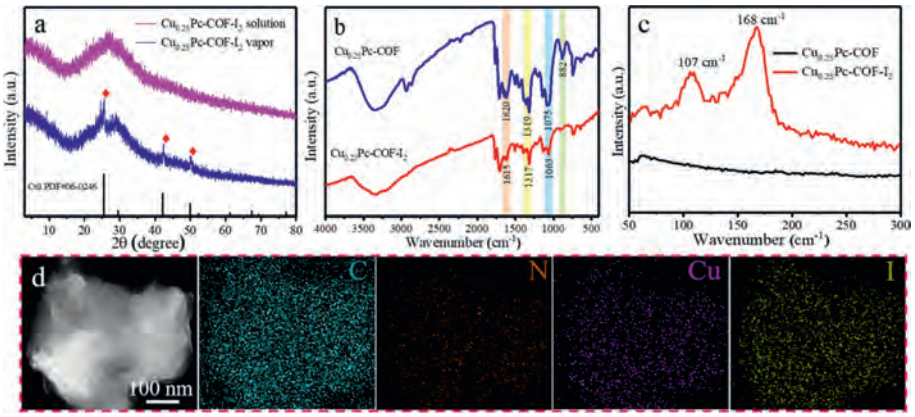

Fig. 3. (a) PXRD patterns of $Cu_{0.25}$Pc-COF adsorbed volatile iodine and iodine-cyclohexane solution. (b) FT-IR and (c) Raman spectra of $Cu_{0.25}$Pc-COF before and after volatile iodine adsorption. (d) Elemental mapping images of C, N, Cu and I for I_2-laden $Cu_{0.25}$Pc-COF.

cupancy of pores and the formation of charge-transfer complexes in the skeleton [8,33].

Through FT-IR spectral analysis, we further explored the interaction mechanism of Cu_xPc-COFs for iodine. There were some changes in the infrared adsorption peak positions of $Cu_{0.25}$Pc-COF after adsorption (Fig. 3b). Notably, the aromatic C−H and C−C bonds stretching vibration peaks of $Cu_{0.25}$Pc-COF at 882 and 1446 cm^{-1} almost disappeared after adsorption. What's more, the C=N band shifted from 1620 cm^{-1} to 1615 cm^{-1}, and the C−N bands at 1319 and 1075 cm^{-1} shifted to 1317 and 1063 cm^{-1}. Similar results were found in the FT-IR spectra of I_2 loading $Cu_{0.5}$Pc-COF and $Cu_{0.125}$Pc-COF materials (Fig. S8 in Supporting information), demonstrating that the adsorption sites were distributed on imine linkage, pyrrole ring and benzene ring of Cu_xPc-COFs [27,36]. Raman spectroscopy measurements were conducted in order to study the species of iodine in $Cu_{0.25}$Pc-COF after adsorption. In the Raman spectrum of I_2-laden $Cu_{0.25}$Pc-COF (Fig. 3c), it was obvious that two strong peaks appeared in the low-frequency spectral region. The peak at ~168 cm^{-1} was confirmed to be the characteristic peak of I_5^- ions, and the peak at ~107 cm^{-1} was assigned to I_3^- ions [8,36]. The generation of polyiodide anions [I_x^-] implied that I_2 was converted into I_3^- or I_5^- during the adsorption process, further revealing that the charge transfer occurred between guest iodine molecules and COFs. As anticipated by the SEM image (Fig. S9 in Supporting information), I_2-laden $Cu_{0.25}$Pc-COF retained the irregular granular crystal morphology but exhibited a rough surface. Furthermore, the corresponding EDS mapping images of C, N, Cu and I were recorded by using HRTEM. The yellow color area in Fig. 3d showed the homogeneous distribution of I element in the I_2-laden $Cu_{0.25}$Pc-COF.

The surface chemical composition and the state of the elements of $Cu_{0.25}$Pc-COF were analyzed by X-ray photoelectron spectroscopy (XPS) measurement. One can see from Fig. 4a, the XPS survey spectrum of I_2-laden $Cu_{0.25}$Pc-COF revealed the presence of iodine characteristic peaks, indicating that iodine species were successfully adsorbed on the sample. The high-resolution XPS spectra of I 3d, C 1s, N 1s and Cu 2p provided more detailed information for clarifying the interaction mechanism. Fig. 4b showed that there were two main characteristic peaks attributed to I_3^- (630.3 and 618.8 eV) and two smaller shoulder peaks assigned to I_2 (631.8 and 620.4 eV) in I 3d XPS spectrum, indicating that the adsorbed iodine species existed in the form of I_2 and I_3^-. Notably, the adsorbed iodine in the $Cu_{0.25}$Pc-COF could further transform into polyiodide anions [I_x^-] due to the charge transfer between I_2 and benzene rings or nitrogen atoms on the imine bonds [52]. As a result, the ratio of I_2/I_3^- was approximately 0.246:1. Deconvolution of the C 1s signal generated three peaks located at 284.7, 286.0 and 287.6

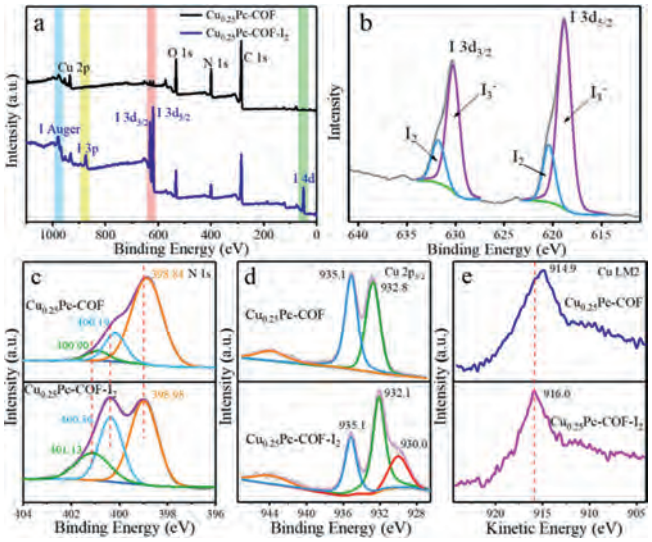

Fig. 4. XPS spectra of $Cu_{0.25}$Pc-COF before and after iodine vapor adsorption: (a) full survey scan, (b) I 3d, (c) N 1s, (d) Cu $2p_{3/2}$ and (e) Cu LM2.

eV, assignable to C=C/C-C, C=N and C=O [53,54], respectively (Fig. S10 in Supporting information). The results agreed well with the expected structure compositions [55], which also verified the existence of the conjugated structure represented by (001) facet in the PXRD pattern. Besides, in the C 1s spectrum of I_2-laden $Cu_{0.25}$Pc-COF, the binding energy of the C=N peak shifted to higher binding energy slightly. Furthermore, the N 1s spectra of $Cu_{0.25}$Pc-COF before and after iodine adsorption were further analyzed. The N 1s spectrum was deconvoluted into three peaks at 398.84, 400.19 and 400.90 eV, which were attributed to corresponding imine linkages (C=N), pyrrolic-N (C=N···Cu) and graphitic-N, respectively (Fig. 4c) [30,53,54]. After iodine adsorption, the shape of the N 1s spectrum was definitely different. The three peaks all shifted slightly to higher binding energy (398.98, 400.36 and 401.13 eV), indicating the strong interaction between N atoms and iodine. More importantly, the high content of nitrogen (10.12 wt%) was exactly the main reason for the excellent iodine absorption capacity [52]. Combined with the results of I 3d spectrum, it could be deduced that the charge-transfer complexes formed between the electron-rich nitrogen-containing groups and iodide [50,56], which was consistent with the results of Raman spectra analysis. In the Cu $2p_{3/2}$ XPS spectrum of $Cu_{0.25}$Pc-COF (Fig. 4d), the peaks at 935.1 and 932.8 eV were assigned to Cu(II) of phthalocyanine structure and

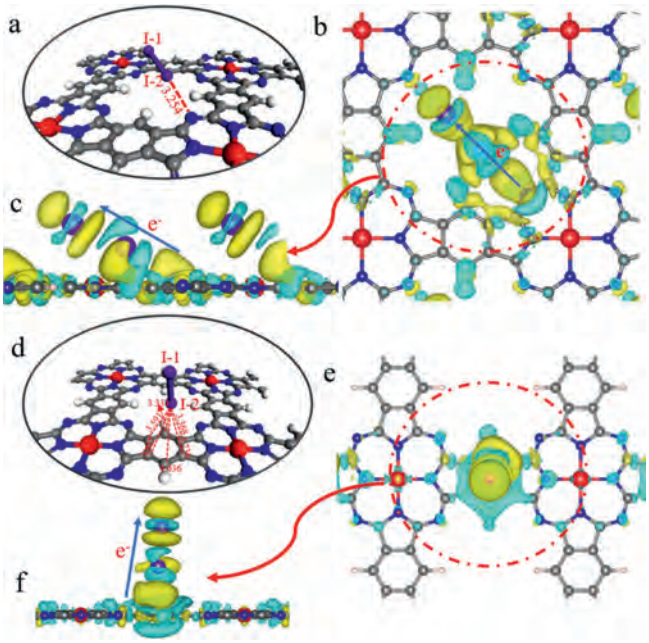

Fig. 5. (a) The optimized structure and (b, c) differential charge density of Cu_xPc-COFs/I_2 complexes on the imine bond. And (d) the optimized structure and (e, f) differential charge density of Cu_xPc-COFs/I_2 complexes on the benzene ring. Colors: I, purple; C, grey; N, blue; Cu, red; H, white. The yellow and blue bubbles represented negative and positive charges, respectively.

Cu(0) [57,58], respectively, which proved that there were two existing states in the sample. A broad peak between 940 eV and 945 eV was the satellite peak accompanied by Cu(II). The results suggested that the chelating center was Cu(II) in the structure of $Cu_{0.25}$Pc-COF. Interestingly, the characteristic Cu(II) peak remained after adsorbing iodine vapor. However, a new peak accompanied with a shoulder peak appeared at 932.1 and 930.0 eV, manifesting the formation of Cu(I) species in the iodide adsorption process [9]. In addition, as the binding energies of Cu(I) and Cu(0) peaks were similar, the Cu LM2 Auger spectra were utilized to further determine the existence of Cu(I) [59]. As shown in Fig. 4e, it was significant that the Cu LM2 Auger peak changed from 914.9 eV to 916.0 eV, which further confirmed the formation of CuI during the adsorption process [58]. The above analysis was consistent with the results of the PXRD investigation.

DFT calculations were carried out to get further insight about the interaction mechanism between iodine and Cu_xPc-COFs. In this part, I_2 was used as fundamental guest iodine to investigate the active sites on the skeleton. The optimized geometries of Cu_xPc-COFs were illustrated in Fig. 5. The calculation results showed that when I_2 was located near the N atom of the imine bond, the distance between I-2 atom and N atom was 3.254 Å, and the corresponding calculated adsorption energy was −22.42 kcal/mol, which was the most stable interaction configuration between I_2 and Cu_xPc-COFs (Fig. 5a). This phenomenon showed that the N atom of the imine bond played a significant role in attracting iodine. The charge number of the N atom decreased after iodine loading, which proved that N atom of the imine bond possessed a strong tendency to donate negative charges. On the other hand, I_2 tilt heavily when it interacted with benzene ring, and the corresponding adsorption energy was −15.41 kcal/mol (Fig. 5d). As a π-conjugated system, benzene ring has rich conjugated electron clouds, which is very beneficial to interact with iodine. The differential charge density plots were shown in Figs. 5b, c, e and f, the yellow and blue regions represented negative and positive charges, respectively. There was obviously charge transfer between I_2 and imine bonds or benzene rings. In detail, imine bonds and benzene rings provided iodine with many negative charges, which eventually accumulated on the I-1 atom. Hence, I_2 could obtain the charge to form polyiodide anions [I_x^-]. Briefly, the N atoms of imine bonds and benzene rings on the skeleton of Cu_xPc-COFs were the main active sites for charge transfer with I_2.

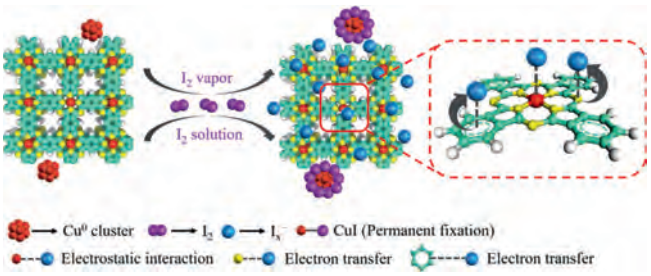

Fig. 6. Schematic illustration of the iodine interaction mechanism of Cu_xPc-COFs. Colors: C, green; N, yellow; Cu, red; H, white.

Taken together, the possible interaction mechanism of iodine enrichment on Cu_xPc-COFs is proposed (Fig. 6). On the basis of FT-IR, Raman, XPS and DFT calculations analyses, Cu_xPc-COFs possessed nitrogen-rich frameworks and electron-rich π-conjugated systems, which could provide abundant active sites for iodine capture. An additional strong driving force for adsorption was the electrostatic interaction between polyiodide anions [I_x^-] and Cu(II) in the center of phthalocyanine structure. The charge transfer and electrostatic interaction were favorable to iodine adsorption process. It could not be neglected that a small amount of Cu° nanoparticles in the sample played the role of permanent trapping of iodine. Here the interaction mechanism has great guiding significance for the specific design and large-scale preparation of highly efficient adsorbent materials to capture iodine.

In summary, we explored a simple microwave method for synthesizing a series of two-dimensional copper-based phthalocyanine-covalent organic frameworks. Due to the high nitrogen content (10.12 wt%) and electron-rich π-conjugated systems, the obtained $Cu_{0.25}$Pc-COF showed excellent iodine uptake capacities of 2.99 g/g for volatile iodine and 492.27 mg/g for the iodine-cyclohexane solution, which are superior to that of most reported porous adsorbents. The adsorption kinetics accorded with the pseudo-second-order kinetic model, suggesting the essence of chemisorption. Meanwhile, the initial adsorption rate reaches ~325.06 mg g^{-1} h^{-1}, indicating the high affinity of $Cu_{0.25}$Pc-COF toward iodine. Combined with experimental data, spectroscopic analyses and theoretical calculations, there are three interaction mechanisms of iodine adsorption: (1) charge-transfer between nitrogen atoms on the imine bonds/electron-rich π-conjugated systems and iodine molecules; (2) electrostatic interaction of Cu-N_4 structures with polyiodide anions (I_x^-); and (3) the trace redox reaction (CuI). Due to the combination of these interactions, Cu_xPc-COFs possess excellent adsorption performance and show great potential as an efficient adsorbent to capture and store radioactive iodine. We believe that the strategy for designing covalent organic frameworks with abundant accessible active single metal centers might open up opportunities in using Cu_xPc-COFs for sensors, energy storage and photoelectrocatalysis.

Declaration of competing interest

The authors declare the following financial interests/personal relationships which may be considered as potential competing interests

Acknowledgments

The authors gratefully acknowledge the financial support from the National Key Research and Development Program of China (No. 2018YFC1900105), the National Natural Science Foundation of China (Nos. U2067215, 22076044), Science Challenge Project (No. TZ2016004), and Beijing Outstanding Young Scientist Program. We also acknowledge Pro. Zhonghua Xiang for helpful discussions.

Supplementary materials

Supplementary material associated with this article can be found, in the online version, at doi:10.1016/j.cclet.2022.03.001.

References

[1] H. Yang, X. Liu, M. Hao, et al., Adv. Mater. (2021) 2106621.
[2] S. Li, Y. Hu, Z. Shen, et al., Sci. China Chem. 64 (2021) 1323–1331.
[3] W. Xie, D. Cui, S.R. Zhang, Y.H. Xu, D.L. Jiang, Mater. Horiz. 6 (2019) 1571–1595.
[4] P. Wang, Q. Xu, Z. Li, et al., Adv. Mater. 30 (2018) 1801991.
[5] S. Xu, S.P.H.T. Freeman, X. Hou, et al., Environ. Sci. Technol. 47 (2013) 10851–10859.
[6] A. Ohtsuru, K. Tanigawa, A. Kumagai, et al., Lancet 386 (2015) 489–497.
[7] K.W. Chapman, P.J. Chupas, T.M. Nenoff, J. Am. Chem. Soc. 132 (2010) 8897–8899.
[8] C. Wang, Y. Wang, R. Ge, et al., Chem. Eur. J. 24 (2018) 585–589.
[9] T.J. Robshaw, S.M. Griffiths, A. Canner, et al., Chem. Eng. J. 390 (2020) 124647.
[10] B. An, J. Zhang, K. Cheng, et al., J. Am. Chem. Soc. 139 (2017) 3834–3840.
[11] X. Meng, S.Y. Song, X.Z. Song, et al., Chem. Commun. 51 (2015) 8150–8152.
[12] A. Beheshti, E.S. Mousavi Fard, M. Kubicki, et al., CrystEngComm 21 (2019) 251–262.
[13] K. Kosaka, M. Asami, N. Kobashigawa, et al., Water. Res. 46 (2012) 4397–4404.
[14] K.S. Subrahmanyam, D. Sarma, C.D. Malliakas, et al., Chem. Mater. 27 (2015) 2619–2626.
[15] G. Lin, L. Zhu, T. Duan, et al., Chem. Eng. J. 378 (2019) 122181.
[16] J.H. Yang, Y.J. Cho, J.M. Shin, M.S. Yim, J. Nucl. Mater. 465 (2015) 556–564.
[17] D.F. Sava, M.A. Rodriguez, K.W. Chapman, et al., J. Am. Chem. Soc. 133 (2011) 12398–12401.
[18] S. Yu, H. Pang, S. Huang, et al., Sci. Total Environ. 800 (2021) 149662.
[19] Z.J. Yin, S.Q. Xu, T.G. Zhan, et al., Chem. Commun. 53 (2017) 7266–7269.
[20] A.P. Côté, A.I. Benin, N.W. Ockwig, et al., Science 310 (2005) 1166–1170.
[21] G. Cheng, A. Zhang, Z. Zhao, et al., Sci. Bull. 66 (2021) 1996–2001.
[22] X. Liu, H. Pang, X. Liu, et al., Innovation 2 (2021) 100076.
[23] M. Bhadra, S. Kandambeth, M.K. Sahoo, et al., J. Am. Chem. Soc. 141 (2019) 6152–6156.
[24] C.O. Kappe, Angew. Chem. Int. Ed. 43 (2004) 6250–6284.
[25] N.L. Campbell, R. Clowes, L.K. Ritchie, A.I. Cooper, Chem. Mater. 21 (2009) 204–206.
[26] X. Qian, Z.Q. Zhu, H.X. Sun, et al., ACS Appl. Mater. Inter. 8 (2016) 21063–21069.
[27] Z. Yan, Y. Yuan, Y. Tian, D. Zhang, G. Zhu, Angew. Chem. Int. Ed. 54 (2015) 12733–12737.
[28] P. Peng, L. Shi, F. Huo, et al., ACS Nano 13 (2019) 878–884.
[29] P. Kuhn, M. Antonietti, A. Thomas, Angew. Chem. Int. Ed. 47 (2008) 3450–3453.
[30] J.H. Park, C.H. Lee, J.M. Ju, et al., Adv. Funct. Mater. 31 (2021) 2101727.
[31] Q. Jiang, H. Huang, Y. Tang, Y. Zhang, C. Zhong, Ind. Eng. Chem. Res. 57 (2018) 15114–15121.
[32] P. Kuhn, A. Forget, D. Su, A. Thomas, M. Antonietti, J. Am. Chem. Soc. 130 (2008) 13333–13337.
[33] L. He, L. Chen, X. Dong, et al., Chem 7 (2021) 699–714.
[34] H.L. Qian, C.X. Yang, X.P. Yan, Nat. Commun. 7 (2016) 12104.
[35] M. Outokesh, A. Saket, S.J. Ahmadi, M. Hosseinpour, A.R. Khanchi, Ind. Eng. Chem. Res. 51 (2012) 15315–15323.
[36] X. Guo, Y. Tian, M. Zhang, et al., Chem. Mater. 30 (2018) 2299–2308.
[37] Y. Liao, J. Weber, B.M. Mills, Z. Ren, C.F.J. Faul, Macromolecules 49 (2016) 6322–6333.
[38] B. Valizadeh, T.N. Nguyen, B. Smit, K.C. Stylianou, Adv. Funct. Mater. 28 (2018) 1801596.
[39] Q. Zhao, L. Zhu, G. Lin, et al., ACS Appl. Mater. Inter. 11 (2019) 42635–42645.
[40] H. Chen, L. Fan, X. Zhang, L. Ma, ACS Appl, Mater. Inter. 12 (2020) 27803–27811.
[41] C. Pei, T. Ben, S. Xu, S. Qiu, J. Mater. Chem. A 2 (2014) 7179–7187.
[42] P. Chen, X. He, M. Pang, et al., ACS Appl. Mater. Inter. 12 (2020) 20429–20439.
[43] D.F. Sava, K.W. Chapman, M.A. Rodriguez, et al., Chem. Mater. 25 (2013) 2591–2596.
[44] T. Geng, W. Zhang, Z. Zhu, et al., Polym. Chem. 9 (2018) 777–784.
[45] A. Sigen, Y.W. Zhang, Z.P. Li, et al., Chem. Commun. 50 (2014) 8495–8498.
[46] Y. Chen, H. Sun, R. Yang, et al., J. Mater. Chem. A 3 (2015) 87–91.
[47] Y. Zhu, Y.-J. Ji, D.G. Wang, et al., J. Mater. Chem. A 5 (2017) 6622–6629.
[48] H. Li, X. Ding, B.H. Han, Chem. Eur. J. 22 (2016) 11863–11868.
[49] F. Yu, Y. Chen, Y. Wang, C. Liu, J. Qin, J. Mater. Res. 35 (2020) 299–311.
[50] Y. Xu, H. Yu, B. Shi, et al., ACS Appl. Polym. Mater. 2 (2020) 3704–3713.
[51] B. Qi, Y. Liu, T. Zheng, et al., J. Solid. State. Chem. 258 (2018) 49–55.
[52] K.Z. Su, W.J. Wang, B.B. Li, D.Q. Yuan, ACS Sustain. Chem. Eng. 6 (2018) 17402–17409.
[53] Z. Meng, R.M. Stolz, K.A. Mirica, J. Am. Chem. Soc. 141 (2019) 11929–11937.
[54] M.D. Zhang, D.H. Si, J.D. Yi, et al., Small 16 (2020) 2005254.
[55] M.C. Wang, M. Ballabio, M. Wang, et al., J. Am. Chem. Soc. 141 (2019) 16810–16816.
[56] C. Xie, J. Song, H. Wu, et al., Green Chem. 20 (2018) 4655–4661.
[57] S. Yan, X. Guan, H. Li, et al., J. Am. Chem. Soc. 141 (2019) 2920–2924.
[58] M.C. Biesinger, Surf. Interface Anal. 49 (2017) 1325–1334.
[59] P. Liu, E.J.M. Hensen, J. Am. Chem. Soc. 135 (2013) 14032–14035.